

## A computational framework to predict post-treatment outcome for gait-related disorders

Jeffrey A. Reinbolt<sup>a</sup>, Raphael T. Haftka<sup>a</sup>, Terese L. Chmielewski<sup>b</sup>,  
Benjamin J. Fregly<sup>a,c,d,\*</sup>

<sup>a</sup> Department of Mechanical & Aerospace Engineering, University of Florida, Gainesville, FL, United States

<sup>b</sup> Department of Physical Therapy, University of Florida, Gainesville, FL, United States

<sup>c</sup> Department of Biomedical Engineering, University of Florida, Gainesville, FL, United States

<sup>d</sup> Department of Orthopaedics and Rehabilitation, University of Florida, Gainesville, FL, United States

Received 5 May 2006; received in revised form 9 May 2007; accepted 9 May 2007

### Abstract

Clinicians often use intuitive models based on clinical experience or regression models based on population studies to plan treatment of gait-related disorders. Because such models are constructed using data collected from previous patients, the predicted clinical outcome for a particular patient may not be reliable. We propose a new approach that uses computational models based on engineering mechanics to predict post-treatment outcome from pre-treatment movement data. The approach utilizes a four-phase optimization process built around a dynamic, patient-specific gait model. The first three phases calibrate the model's joint, inertial, and control parameters, respectively, where the control parameters are weights in an optimization cost function that tracks the patient's pre-treatment gait motion and loads. The last phase predicts the patient's post-treatment gait pattern by performing a tracking optimization with the calibrated model modified to simulate the selected treatment.

We demonstrate the approach by simulating how two treatments for knee osteoarthritis (OA) – gait modification and high tibial osteotomy (HTO) surgery – alter the external knee adduction torque for a specific patient. By performing multiple tracking optimizations, we calibrated the model's parameter values to reproduce the patient's knee adduction torque curve for a toe out gait motion. When we performed a tracking optimization with the calibrated model using a modified footpath to simulate an increased stance width, the predicted reduction in both adduction torque peaks matched experimental results to within 4.8% error. When we performed a tracking optimization with the same model using modified leg geometry to simulate HTO surgery, the predicted reductions were consistent with published data. The approach requires further evaluation with a larger number of patients to determine its effectiveness for planning the treatment of gait-related disorders on a patient-specific basis.

© 2007 IPPEM. Published by Elsevier Ltd. All rights reserved.

**Keywords:** Patient-specific; Optimization; Gait; Knee adduction moment; High tibial osteotomy

### 1. Introduction

Clinicians would like to predict post-treatment clinical outcome on an individual patient basis given the treatment approach and parameters under consideration. Two exam-

ples related to knee osteoarthritis (OA) treatment are gait modification and high tibial osteotomy (HTO) surgery. In both cases, the goal is to shift the weight-bearing axis of the leg (i.e., hip center to ankle center) from the diseased medial to the healthy lateral compartment of the knee. This shift alters the medial–lateral load distribution in the knee, slowing or possibly even reversing the degenerative disease process.

The external knee adduction torque measured during post-treatment gait has been identified as a quantitative indicator of long-term clinical outcome [1–5]. This quantity has recently

\* Corresponding author at: Department of Mechanical & Aerospace Engineering, 231 MAE-A Building, P.O. Box 116250, University of Florida, Gainesville, FL 32611-6250, United states. Tel.: +1 352 392 8157; fax: +1 352 392 7303.

E-mail address: [fregly@ufl.edu](mailto:fregly@ufl.edu) (B.J. Fregly).

been shown to be highly correlated with *in vivo* medial compartment load during gait [6]. Though the knee adduction torque can also be measured pre-treatment, it is not normally used for treatment planning. Instead, clinicians use experience and clinical observations to determine the best treatment approach and parameters. Unfortunately, clinical outcomes from HTO surgery have been highly variable, and identification of novel gait patterns that offload the medial compartment has been elusive.

Since clinical experience alone has not led to optimal outcomes, previous studies have used experimental and computational methods to seek to identify optimal treatment approaches. For gait modifications, experimental studies have investigated how changes in stride length [5], walking speed [7], and toe out angle [1,5,8,9] affect the peak knee adduction torque. For HTO surgery, gait studies [2,4,5], cadaver studies [10,11], and computer modeling studies [12,13] have investigated how surgical method (e.g., opening versus closing wedge) and parameters affect the medial–lateral load distribution in the knee following surgery. While these studies have led to general principles for altering the load distribution, no quantitative method currently exists for accurately predicting how a particular intervention will affect the post-treatment knee adduction torque for an individual patient.

This study presents a novel computational framework for predicting post-treatment functional outcome from pre-treatment movement data on an individual patient basis. The foundation of the framework is a three-dimensional, 27 degree-of-freedom (DOF), full-body gait model. The framework utilizes a four-phase optimization procedure. The first three phases calibrate the model's joint parameters (JPs: positions and orientations of joint axes in the body segment coordinate systems), inertial parameters (IPs: body segment masses, mass centers, and central principal moments of inertia), and control parameters (CPs: tracking weights in an optimization cost function) to the patient's pre-treatment movement data. The last phase uses the calibrated model to predict the patient's post-treatment outcome. We demonstrate the framework by simulating how gait modification and HTO surgery alter the knee adduction torque in a specific patient. The predictions are compared to adduction torque changes measured experimentally for a modified gait pattern performed by the same patient and reported in the literature for HTO surgery.

## 2. Methods

### 2.1. Experimental data

Experimental kinematic and ground reaction data were collected from a single patient with knee OA (male, age 41 years, height 170 cm, mass 69 kg, alignment 5° varus) using a video-based motion analysis system (Motion Analysis Corporation, Santa Rosa, CA) and two force plates (AMTI, Watertown, MA). Institutional review board approval and

informed consent were obtained prior to the experiments. Comparable to Reinbolt et al. [14], the Cleveland Clinic marker set was used with 2 additional markers (e.g., superior and lateral) placed on each hindfoot segment for a total of 37 markers. Eight static markers over the medial and lateral femoral epicondyles and medial and lateral malleoli were used in conjunction with 29 dynamic markers to create segment coordinate systems for the dynamic model described below.

Unloaded isolated joint motion trials were performed to exercise the primary functional axes of each lower extremity joint (i.e., hip, knee, and ankle). For each joint, the patient was instructed to move the distal segment within the physiological range of motion so as to voluntarily exercise all DOFs of the joint. For each hip, multiple cycles of flexion–extension followed by abduction–adduction were recorded. Similar to Leardini et al. [15], internal–external rotation was avoided to reduce skin and soft tissue movement artifacts. For each knee, multiple cycles of knee flexion–extension were recorded. For each ankle, multiple cycles of combined plantarflexion–dorsiflexion and inversion–eversion were recorded.

Gait kinematic and ground reaction data were collected to provide simultaneous motion of all lower extremity joints under load-bearing physiological conditions. One cycle (e.g., left heel strike to left heel strike) of three gait motions with different footpaths (i.e., the position and orientation of each foot with respect to the laboratory coordinate system) was recorded to produce a range of different knee adduction torque curves, where resultant joint torques were computed from inverse dynamics. The first gait motion used the patient's self-selected normal footpath, the second one used a toe out gait motion (i.e., increased foot progression angle), and the third used a wide stance gait motion (i.e., increased width between feet). Marker data were collected at 120 Hz during 10 s for isolated joint motion trials and 5 s for gait motion trials. Raw marker data were filtered using a fourth-order, zero phase-shift, low pass Butterworth Filter with a cutoff frequency of 6 Hz [16].

### 2.2. Dynamic model

The foundation of the proposed computational framework is a three-dimensional, full-body dynamic gait model (Fig. 1). The equations of motion for the 27 DOF model were derived with the symbolic manipulation software Autolev<sup>TM</sup> (OnLine Dynamics, Sunnyvale, CA). Comparable to Anderson and Pandy's [17] model structure, three translational and three rotational DOFs express the movement of the pelvis in the laboratory coordinate system and the remaining 13 segments comprise four open chains branching from the pelvis.

The positions and orientations of joint axes within adjacent segment coordinate systems are defined by unique JPs. For example, a single knee joint axis is simultaneously estab-

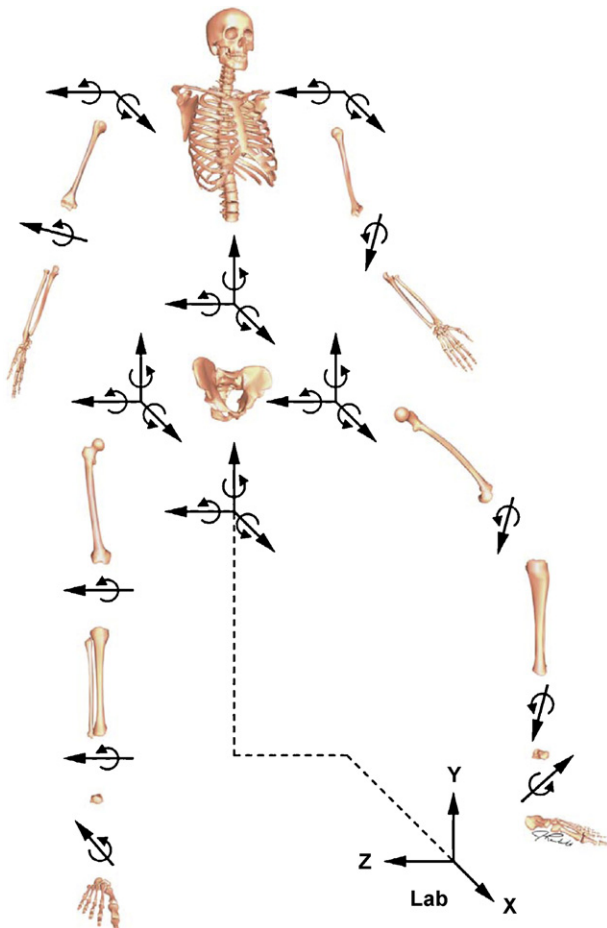


Fig. 1. Schematic of the three-dimensional, 14 segment, 27 DOF full-body model linkage joined by a set of gimbal, universal, and pin joints. The dynamic model forms the foundation for the four-phase optimization process used for the computational framework.

lished in both the femur and tibia coordinate systems. These parameters are used to designate the following joint types: 3 DOF hips, 1 DOF knees (with external adduction torque calculated from the corresponding internal reaction torque), 2 DOF ankles with nonintersecting axes [16], 3 DOF back, 2 DOF shoulders, and 1 DOF elbows. Each joint type provides a simplified mechanical approximation to the primary *in vivo* motions of the corresponding anatomical joint. The masses, mass centers, and central principal moments of inertia for each body segment are defined by unique IPs. Anatomic landmark methods are used to estimate nominal values for JPs [18–20] and IPs [21] based on scaling rules developed from cadaver studies. Nominal values for the JPs are taken from [14], while nominal values for the IPs are determined from the patient's height and weight using regression relationships reported in [21].

### 2.3. Computational framework

Built on the foundation of this dynamic model is a four-phase optimization approach for calibrating model parameter

values and predicting post-treatment outcome with the calibrated model (Fig. 2). All four optimization phases use Matlab's nonlinear least squares algorithm (The Mathworks, Natick, MA). Unless otherwise stated, the derivatives needed by each optimization are calculated analytically using the automatic differentiation program ADOL-C [22].

The first phase calibrates the model's JP values by performing a sequence of optimizations (Fig. 2, Phase 1). First, JP values for individual lower extremity joints are optimized separately using isolated joint motion data, and then JP values for all lower extremity joints are optimized together using a gait motion trial. Each optimization simultaneously adjusts JP values and model motion to track an experimental motion as closely as possible. This single level formulation is different from our previous nested, or two-level, optimization formulation that separated the adjustment of JP values and model motion [14]. The JP cost function ( $e_{JP}$ , Eq. (1)) minimizes errors between the model ( $m'$ ) and experimental ( $m$ ) marker locations over  $nm$  markers, 3 Cartesian coordinates, and  $nf$  time frames:

$$e_{JP} = \min_{p_{JP}, q} \sum_{i=1}^{nf} \sum_{j=1}^3 \sum_{k=1}^{nm} [m_{ijk} - m'_{ijk}(p_{JP}, q)]^2 \quad (1)$$

For all JP optimizations, the design variables are selected lower extremity JP values ( $p_{JP}$ ) along with 540 B-spline nodes ( $q$ ) parameterizing 27 generalized coordinate trajectories defining the model motion with 20 nodes per DOF. The initial seed for each B-spline node is taken as zero, which represents a static model without motion. Optimization of an isolated joint motion trial uses 6 hip, 9 knee, or 12 ankle JP values. In contrast, optimization of the gait motion trial uses a reduced set of 4 hip, 9 knee, and 4 ankle JPs, since determination of certain JP values (e.g., hip joint center location along the medial–lateral axis) is inaccurate for motions of less than  $25^\circ$  (e.g., hip abduction–adduction angle throughout the gait cycle) [23]. Initial JP values for the gait optimization are taken from the isolated joint optimization results.

The second phase calibrates the model's IP values by performing a single optimization (Fig. 2, Phase 2). This calibration step adjusts IP values but not model motion (i.e., optimal gait kinematics are taken from the JP optimization above) to reduce residual loads (i.e., fictitious external forces and torques). These loads are computed from inverse dynamics and exist due to model structure, model parameter value, and experimental measurement errors. At the root of our dynamic model is a non-anatomical 6 DOF ground-to-pelvis joint. Though this joint is not actuated in real life, it requires residual loads to maintain dynamic consistency with the experimental data. The IP cost function ( $e_{IP}$ , Eq. (2)) minimizes a combination of differences between initial ( $p_{IP}$ ) and optimal ( $p_{IP}$ ) IP values and residual loads ( $F$  and  $T$ ) at the ground-to-pelvis joint over 3 Cartesian coordinates

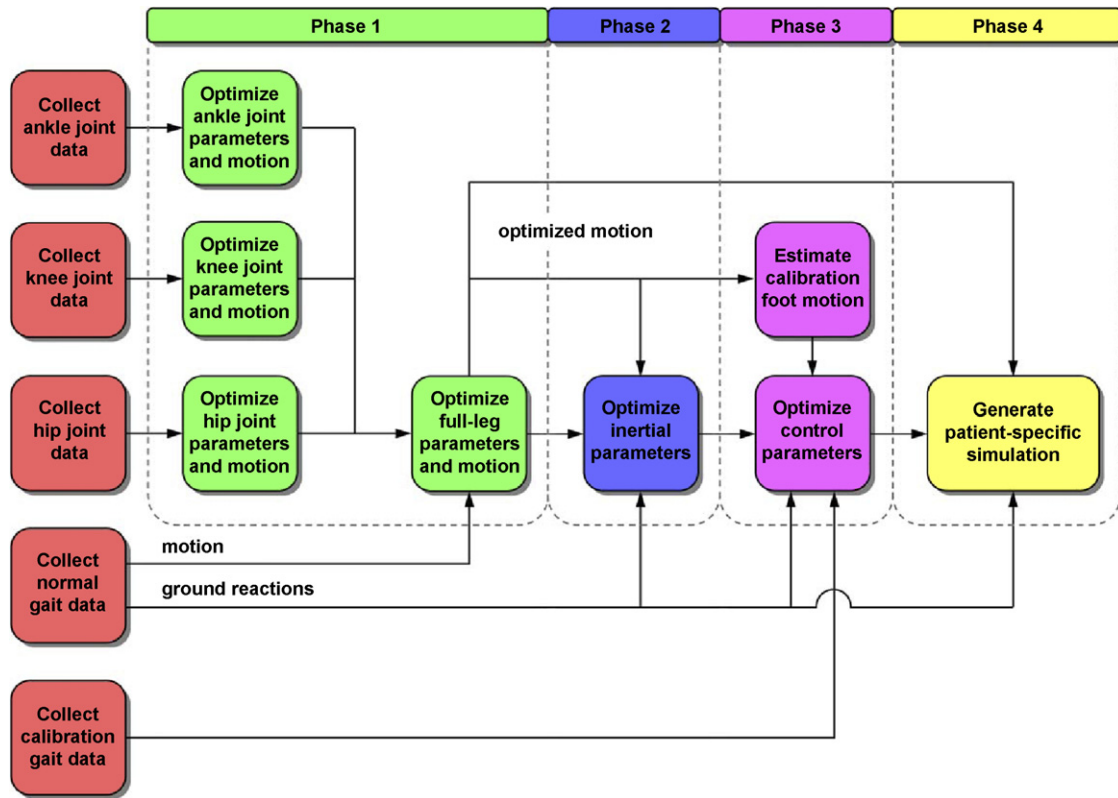


Fig. 2. Flow chart describing the four phases of the optimization process. For phase 1, isolated joint motion and normal gait data are used to calibrate lower extremity joint parameter values under weight bearing conditions. For phase 2, calibrated joint parameter values and normal gait data are used to calibrate full-body inertial parameter values. For phase 3, calibrated joint and inertial parameter values are used along with normal and calibration gait data sets to calibrate control parameter values. For phase 4, the calibrated joint, inertial, and control parameter values are used in an inverse dynamics optimization to predict a patient-specific post-treatment gait pattern.

and  $nf$  time frames:

$$e_{IP} = \min_{p_{IP}} \sum_{i=1}^{nf} \sum_{j=1}^3 \left\{ \left[ \frac{F_{ij}(p_{IP})}{BW} \right]^2 + \left[ \frac{T_{ij}(p_{IP})}{BW \times HT} \right]^2 \right\} + \left( \frac{p_{IP} - p'_{IP}}{p'_{IP}} \right)^2 \quad (2)$$

The design variables are a set of IP values composed of 7 masses, 8 mass center components, and 21 moments of inertia. This set accounts for body symmetry and limited motion of some segments during gait. The initial seed for each IP value is its corresponding nominal value from [21]. Due to kinematic noise, the cost function includes a term that minimizes changes in IP values away from their initial guesses. Without this term, the optimization predicts unrealistic solutions (e.g., negative masses or moments of inertia). Each term in the cost function is normalized to create non-dimensional errors. The residual forces ( $F$ ) on the pelvis are normalized by body weight (BW) and the residual torques ( $T$ ) on the pelvis by body weight  $\times$  height (BW  $\times$  HT). IP changes are normalized by their respective initial values ( $p'_{IP}$ ). Once an IP optimization converges (i.e., cost function value chang-

ing by less than  $1e-3$  in consecutive optimizer steps), the optimal IP values are used as the initial guess for a subsequent IP optimization, with this process being repeated until the resulting residual loads converge (i.e., all residual values changing by less than  $1e-3$  in consecutive IP optimizations). This optimization formulation is very efficient computationally, eliminating the need to form analytical derivatives with automatic differentiation.

The third phase calibrates the model's CP values by performing a two-level optimization (Fig. 2, Phase 3). The outer level optimization adjusts CP values which are used as weight factors in the inner level cost function. When the optimal CP values are found, the inner level optimization predicts a gait motion and associated loads that minimize the cost function of the outer level optimization. This problem formulation requires two sets of gait data—an initial pre-treatment data set to be tracked and a final calibration data set to be predicted. Each data set consists of kinematic and ground reaction data as well as resultant joint torques and pelvis residual loads computed from inverse dynamics.

The inner level optimization performs repeated inverse dynamics analyses of a complete gait cycle (heel strike to subsequent heel strike of the same leg) using the current guess for the CP values along with model or gait data modifica-

tions (e.g., altered leg geometry or footpath) to represent the imposed treatment. The cost function ( $e_{\text{inner}}$ , Eq. (3)) minimizes kinematic and kinetic changes away from the initial gait data over  $nf$  time frames:

$$\begin{aligned}
 e_{\text{inner}} = \min_{\mathbf{q}, \mathbf{r}} \sum_{i=1}^{nf} \left[ w_1 \sum_{j=1}^6 \sum_{k=1}^{ns} (\Delta q_{\text{foot}}^2)_{ijk} + w_2 \sum_{j=1}^2 (\Delta q_{\text{pelvis}}^2)_{ij} \right. \\
 + w_3 \sum_{j=1}^3 (\Delta q_{\text{trunk}}^2)_{ij} + w_4 \sum_{j=1}^2 \sum_{k=1}^{ns} (\Delta \text{CoP}_{\text{foot}}^2)_{ijk} \\
 + w_5 \sum_{j=1}^3 (\Delta F_{\text{pelvis}}^2 + \Delta T_{\text{pelvis}}^2)_{ij} \\
 + \sum_{k=1}^{ns} (w_6 \Delta T_{\text{hip flexion}}^2 + w_7 \Delta T_{\text{hip adduction}}^2 \\
 + w_8 \Delta T_{\text{hip rotation}}^2 + w_9 \Delta T_{\text{knee flexion}}^2 \\
 \left. + w_{10} \Delta T_{\text{ankle dorsiflexion}}^2 + w_{11} \Delta T_{\text{ankle inversion}}^2)_{ik} \right] \quad (3)
 \end{aligned}$$

The design variables are 540 ( $\mathbf{q}$ ) and 120 ( $\mathbf{r}$ ) B-spline nodes parameterizing 27 generalized coordinate and 12 ground reaction trajectories, respectively, with 20 nodes per curve. The initial guess for each B-spline node is the corresponding value from the optimal gait kinematics determined by the first phase JP optimization for  $\mathbf{q}$  and from parameterizing the ground reactions from the same gait trial for  $\mathbf{r}$ . Tracking errors ( $\Delta$ ) between initial and predicted gait data are summed, over both sides ( $ns$ ) where possible, for the following quantities: 6 weighted ( $w_1$ ) footpath translations and rotations ( $q_{\text{foot}}$ ), 2 weighted ( $w_2$ ) pelvis transverse plane translations ( $q_{\text{pelvis}}$ ), 3 weighted ( $w_3$ ) trunk rotations ( $q_{\text{trunk}}$ ), 2 weighted ( $w_4$ ) center of pressure locations ( $\text{CoP}_{\text{foot}}$ ), 3 weighted ( $w_5$ ) ground-to-pelvis residual forces ( $F_{\text{pelvis}}$ ), 3 weighted ( $w_5$ ) ground-to-pelvis residual torques ( $T_{\text{pelvis}}$ ), 1 weighted ( $w_6$ ) hip flexion–extension torque ( $T_{\text{hip flexion}}$ ), 1 weighted ( $w_7$ ) hip adduction–abduction torque ( $T_{\text{hip adduction}}$ ), 1 weighted ( $w_8$ ) hip internal–external rotation torque ( $T_{\text{hip rotation}}$ ), 1 weighted ( $w_9$ ) knee flexion–extension torque ( $T_{\text{knee flexion}}$ ), 1 weighted ( $w_{10}$ ) ankle dorsiflexion–plantarflexion torque ( $T_{\text{ankle dorsiflexion}}$ ), and 1 weighted ( $w_{11}$ ) ankle inversion–eversion torque ( $T_{\text{ankle inversion}}$ ). To eliminate the influence of walking direction on tracking errors, we measure footpath and pelvis kinematics with respect to a pelvis progression coordinate system whose origin is defined as the pelvis origin,  $x$  direction by the initial and final position of the pelvis origin,  $y$  direction as superior, and  $z$  direction as  $x$  cross  $y$ . To permit CoP tracking for altered footpaths, we measure each CoP location on the bottom of the foot with respect to the foot coordinate system. The cost function weight  $w_1$  is set to 10 to provide tight tracking of each footpath while the weights  $w_2$ – $w_5$  are set to

1 to provide loose tracking of those quantities. The remaining cost function weights  $w_6$ – $w_{11}$  on control torque tracking errors define the model's CP values, which keep the predicted torques in the neighborhood of the initial pre-treatment gait data. The predicted gait motion and loads will differ from the initial gait data due to modifications added to the model or pre-treatment gait data to represent the simulated treatment.

The outer level optimization is used to calibrate the CP values that serve as weights in the inner level cost function. Thus, each outer level function evaluation is an inner level optimization. The outer level cost function ( $e_{\text{outer}}$ , Eq. (4)) minimizes the difference between predicted ( $M'$ ) and measured ( $M$ ) quantities of clinical significance (e.g., the external knee adduction torque) over  $nf$  time frames, where predicted quantities are produced by the inner level optimization through tracking of pre-treatment gait data, and measured quantities are taken directly from the calibration gait data:

$$e_{\text{outer}} = \min_{\mathbf{p}_{\text{CP}}} \sum_{i=1}^{nf} [M_i - M'_i(\mathbf{p}_{\text{CP}})]^2 \quad (4)$$

The design variables are 6 CP values ( $\mathbf{p}_{\text{CP}}$ ) defined by weights  $w_6$ – $w_{11}$  on control torque tracking errors in the inner-level cost function (Eq. (3)). Initial CP values are taken as zero. The quantities appearing in the outer level cost function are not tracked by the inner level cost function.

Since repeated inner level optimizations would be extremely costly computationally, we use quadratic response surfaces (RSs) as surrogates for the inner level optimizations. For each time frame  $i$ , the prediction error ( $M_i - M'_i(\mathbf{p}_{\text{CP}})$ ) is fit as a multidimensional quadratic function of the six CP values ( $\mathbf{p}_{\text{CP}}$ ). A quadratic RS with six design variables requires solution of 28 unknown polynomial coefficients. Consequently, we generate a redundant set of 64 six-dimensional CP sample points within the bounds of 0 (i.e., no tracking) to 10 (i.e., tight tracking) using a Hammersley Quasirandom Sequence [24]. We then perform a separate inner level optimization for each of the 64 sample points to characterize the relationship between input CP values and output prediction error at each time frame. Finally, we calculate the 28 RS coefficients for each time frame via linear least squares using Matlab.

Once quadratic RSs are available, we perform multiple outer level optimizations to maximize the likelihood of finding the global minimum. Each time the outer level optimization performs a function evaluation, we call the RS approximations for prediction errors rather than performing an explicit inner level optimization. We repeat the outer level optimization 1000 times using different initial guesses for CP values, again using a Hammersley Quasirandom Sequence to generate values within the bounds of 0–10. The 6 CP values that produce the lowest value of the outer level cost function (Eq. (4)) are used in the calibrated model, and a final explicit inner level optimization is performed with these CP values to predict gait kinematics and kinetics.

The fourth phase of the computational framework predicts the patient's post-treatment functional outcome using the calibrated model with modifications that represent the simulated treatment (Fig. 2, Phase 4). No post-treatment experimental gait data is needed for this phase. Given optimal CP values from the third phase, this phase performs an inverse dynamics gait optimization using the inner level cost function from CP calibration (Eq. (3)). Since the simulated treatment differs from that used for CP calibration, the optimization will predict a new gait pattern. Some simulated treatments may involve kinematic or kinetic changes (e.g., altered footpath) that require the pre-treatment gait data to be modified for tracking purposes. Other simulated treatments may involve changes to model parameters (e.g., HTO surgery) that do not require modification of the pre-treatment gait data used for tracking.

#### 2.4. Framework demonstration

To demonstrate the computational framework, we chose treatment planning for knee OA as a sample application. Two specific treatments were considered, both of which involved prediction of the post-treatment external knee adduction torque for the left leg. The first simulated treatment was gait modification via increased stance width while the second was HTO surgery.

Both simulated treatments were applied to a calibrated model constructed of the patient from whom isolated joint motion and gait data were collected. We calibrated the model's JP and IP values using the patient's isolated joint motion and normal gait data and the model's CP values using the patient's normal (as pre-treatment) and toe out (as calibration) gait data. To approximate toe out gait for CP calibration, we increased each pre-treatment foot progression angle by a constant offset (approximately  $15^\circ$ ) to match the average value measured during toe out gait. We also added small anterior–posterior and medial–lateral translation offsets to each pre-treatment footpath to approximate the patient's toe out footpath as closely as possible using only simple adjustments.

After calibration, the model was used to predict the patient's knee adduction torque curve for the two simulated treatments using the patient's normal gait data as the pre-treatment data set. To simulate gait modification with an increased stance width, we increased the lateral translation of each pre-treatment footpath by a constant offset (approximately 10 cm) to match the average value of the patient's wide stance footpath. We also added small anterior–posterior translation and progression angle offsets to each pre-treatment footpath to approximate the patient's wide stance footpath as closely as possible. The wide stance gait data were not used explicitly in any optimization step. The adduction torque curve predicted by the inverse dynamics tracking optimization was compared to the experimental adduction torque curve measured from the same patient during wide stance gait. To simulate HTO surgery, we left the pre-treatment foot-

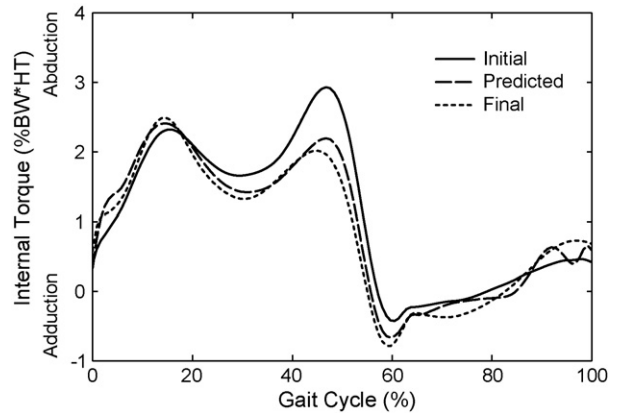


Fig. 3. Comparison of left internal knee abduction torque curves for phase 3 control parameter calibration. Initial (solid line) curve is from the patient's normal gait pattern measured experimentally, predicted (dashed line) curve is from the toe out gait pattern reproduced by the control parameter calibration process, and final (dotted line) curve is from the patient's toe out gait pattern measured experimentally.

path unchanged and instead modified the geometry of the left tibia in a manner consistent with a lateral opening wedge osteotomy. Using standing radiographs from the patient, we defined the anterior–posterior axis of the osteotomy to be 10 cm inferior and 5 cm lateral to the midpoint of the transepicondylar axis. The post-treatment knee adduction torque was simulated for 3, 5, and  $7^\circ$  of correction, and the predictions were compared with data reported in literature for the same corrections [2,25].

### 3. Results

After calibration, the patient-specific model matched the two peaks and the shape of the toe out gait adduction torque curve well (Fig. 3). The first peak was underestimated by  $0.08\% \text{ BW} \times \text{HT}$  and occurred at the correct time in the gait cycle. The second peak was overestimated by  $0.18\% \text{ BW} \times \text{HT}$  and was delayed slightly (1.61% of gait cycle). The root-mean-square (RMS) error in the predicted knee adduction torque curve was  $0.16\% \text{ BW} \times \text{HT}$  over the stance phase. By comparison, the RMS difference between adduction torque curves for the same subject over three separate trials of toe out gait was  $0.21\% \text{ BW} \times \text{HT}$ . The optimal set of CP values varied in magnitude (Table 1), with more tracking weight placed on the hip flexion–extension, ankle dorsiflexion–plantarflexion, and ankle inversion–eversion torques than on the other leg control torques. RMS errors in predicted kinematic and kinetic quantities were within  $6^\circ$  for joint angles, roughly 10 mm for centers of pressure, between 0.21 and  $0.76\% \text{ BW} \times \text{HT}$  for joint torques, and less than 5% BW for ground reaction forces (Table 2, Toe Out).

When the calibrated model was used to predict the knee adduction torque for the patient's wide stance gait pattern, the peak values agreed better than did the shape of the curve between the peaks (Fig. 4). The first peak was overestimated

Table 1

Chosen ( $w_1$ – $w_5$ ) and calibrated ( $w_6$ – $w_{11}$ ) tracking weights used in the inner level inverse dynamics optimization cost function (Eq. (3))

| Variable | Value |
|----------|-------|
| $w_1$    | 10.00 |
| $w_2$    | 1.00  |
| $w_3$    | 1.00  |
| $w_4$    | 1.00  |
| $w_5$    | 1.00  |
| $w_6$    | 5.17  |
| $w_7$    | 0.36  |
| $w_8$    | 1.08  |
| $w_9$    | 0.29  |
| $w_{10}$ | 5.55  |
| $w_{11}$ | 9.17  |

The calibrated weights are determined in the third phase of the computational framework.

by 0.10% BW  $\times$  HT and was delayed slightly (2.42% of gait cycle). The second peak was overestimated by 0.02% BW  $\times$  HT and occurred slightly early (0.81% of gait cycle). The RMS error in the predicted knee adduction torque curve was 0.24% BW  $\times$  HT over the stance phase. By comparison, the RMS difference between adduction torque curves for the same subject over three separate trials of wide stance gait was 0.23% BW  $\times$  HT. RMS errors in predicted kinematic and kinetic quantities were within 5° for joint angles, on the order of 10 mm for centers of pressure, between 0.24 and 0.52% BW  $\times$  HT for joint torques, and less than 5% BW for ground reaction forces (Table 2, Wide Stance).

When the calibrated model was used to predict the patient's knee adduction torque following simulated HTO surgery, the peak values decreased as the angle of correction increased (Fig. 5). The first peak decreased nonlinearly

Table 2

Root-mean-square (RMS) errors during stance phase between patient-specific toe out and wide stance gait predictions generated using the computational framework and toe out and wide stance gait measurements made on the same patient

| Quantity                                 | RMS error |             |
|--|-----------|-------------|
|  | Toe Out   | Wide Stance |
| Hip flexion angle (°)                    | 3.11      | 4.25        |
| Hip abduction angle (°)                  | 2.63      | 2.37        |
| Hip rotation angle (°)                   | 5.73      | 2.79        |
| Knee flexion angle (°)                   | 2.58      | 2.68        |
| Ankle flexion angle (°)                  | 2.96      | 4.79        |
| Ankle inversion angle (°)                | 4.45      | 3.91        |
| Anterior center of pressure (mm)         | 13.24     | 10.49       |
| Lateral center of pressure (mm)          | 9.22      | 10.97       |
| Hip flexion torque (%BW $\times$ HT)     | 0.76      | 0.52        |
| Hip abduction torque (%BW $\times$ HT)   | 0.38      | 0.35        |
| Hip rotation torque (%BW $\times$ HT)    | 0.21      | 0.28        |
| Knee flexion torque (%BW $\times$ HT)    | 0.25      | 0.40        |
| Knee adduction torque (%BW $\times$ HT)  | 0.16      | 0.24        |
| Ankle flexion torque (%BW $\times$ HT)   | 0.69      | 0.49        |
| Ankle inversion torque (%BW $\times$ HT) | 0.48      | 0.45        |
| Anterior ground reaction force (%BW)     | 1.74      | 1.30        |
| Superior ground reaction force (%BW)     | 5.06      | 4.92        |
| Lateral ground reaction force (%BW)      | 0.41      | 2.25        |

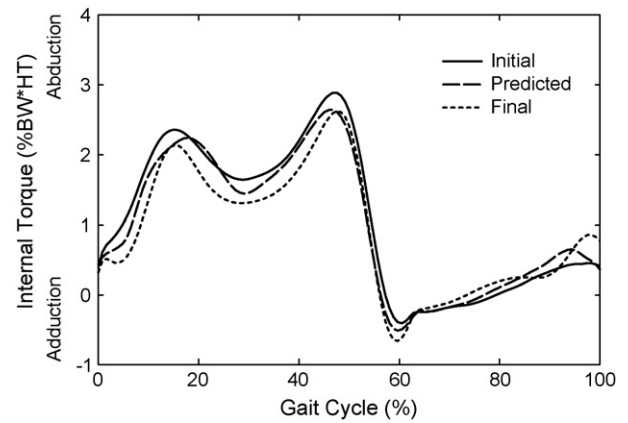


Fig. 4. Comparison of left internal knee abduction torque curves for phase 4 prediction of treatment outcome due to gait modification with increased stance width. Initial (solid line) curve is from the patient's normal gait pattern measured experimentally, predicted (dashed line) curve is from the wide stance gait pattern predicted by the calibrated patient-specific optimization, and final (dotted line) curve is from the patient's wide stance gait pattern measured experimentally.

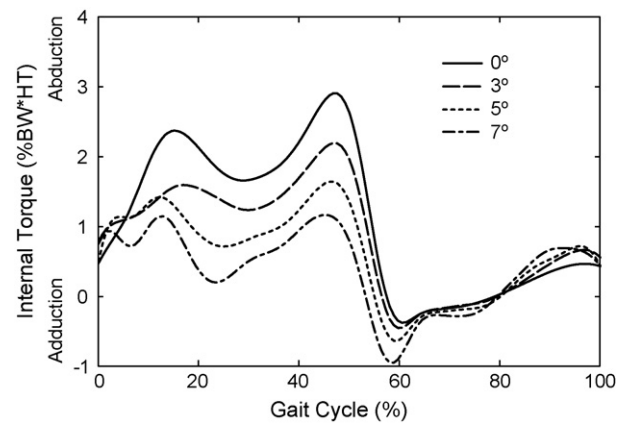


Fig. 5. Comparison of left internal knee abduction torque curves for phase 4 prediction of treatment outcome due to simulated opening wedge high tibial osteotomy. 0° (solid line) curve is from the patient's normal gait pattern measured experimentally, and 3° (dashed line), 5° (dotted line), and 7° (dashed-dotted line) curves are from the post-surgery gait patterns predicted by the calibrated patient-specific optimization for three levels of angular correction.

and the second peak approximately linearly as a function of angular correction amount. Compared with adduction torque changes following HTO surgery reported in the literature [2,25], the peak value decreased by 0.71% BW  $\times$  HT for the 3° case (versus 1.1% BW  $\times$  HT in [2]), 1.2% BW  $\times$  HT for the 5° case (versus 1.3% BW  $\times$  HT in [2]), and 1.7% BW  $\times$  HT for the 7° case (versus 1.6% BW  $\times$  HT in [2]).

#### 4. Discussion

This study presented a novel computational framework to predict post-treatment gait changes given pre-treatment gait data for a specific patient. The framework utilizes a

four-phase optimization approach to calibrate a dynamic, full-body gait model to a patient's movement data and then use the calibrated model to predict post-treatment functional outcome. The framework was demonstrated by predicting changes in the external knee adduction torque as observed experimentally for different gait motions or reported in the literature for HTO surgery. Though the approach was successful for one patient and the current data sets, simulation of a larger number of patients and wider variety of treatments is needed to evaluate the approach more fully. In particular, a full evaluation of our simulated HTO results would require gait testing of a patient before and after HTO surgery, which is difficult in the United States since few surgeons continue to perform this procedure.

The current computational framework has several limitations related to assumptions in both the model and the methodology. For the model, a pin joint knee was chosen to represent the primary flexion–extension motion that dominates secondary knee motions during gait. To eliminate the effect of this approximation on the calculated knee adduction torque, we use only the foot and shank from the full-body model to calculate an unconstrained adduction torque curve. We then place a large weight on shank segment marker coordinate errors to ensure that the curve produced by the full-body model with pin joint knee matches the curve produced by the foot-shank model with unconstrained knee. A rigid foot model without an explicit ground contact model was selected to increase computational speed and exploit the ability to prescribe a desired footpath for the inverse dynamics optimization. For the methodology, the primary assumption is that after treatment, the patient will move in a manner similar to before treatment, thereby motivating the need for pre-treatment movement data to be tracked.

Toe out gait was selected for CP calibration to obtain the largest change in knee adduction torque compared to the normal gait pattern. If we had chosen wide stance gait instead for CP calibration, we would have likely obtained different CP values since the changes in the knee adduction torque curve relative to normal gait were less pronounced. Furthermore, the CP values identified in phase three depend on the weights chosen for the other tracking terms. For example, if the weight on center of pressure tracking errors was calibrated as well, the calibrated weights for control torque tracking would likely change. Although referred to as control parameters, the calibrated cost function weights do not have an obvious physical interpretation tied to neural control strategies. Nonetheless, it appears reasonable to assume that the patient's post-treatment gait pattern will be a neighboring solution to the pre-treatment gait pattern. Furthermore, the motion for CP calibration must be chosen such that an envelope of feasible joint torques is produced that contains a neighborhood of motions large enough to result in the predicted motion.

The necessary phases of the computational framework vary depending on the particular treatment planning application. It is possible to remove JP calibration, IP calibration, and/or CP calibration from the workflow, replacing omitted

phases with parameter values obtained from anatomical landmark methods (JP and IP values) or with all ones (CP values). When we removed JP calibration from the workflow, we were unable to find CP values that could accurately reproduce the toe out and wide stance gait adduction torque curves. In contrast, when we removed IP calibration from the workflow, the decrease in prediction accuracy was small for both gait patterns. These findings are consistent with a recent Monte Carlo analysis we performed, where we found that inverse dynamics results from our patient-specific model are sensitive to errors in JP but not IP values [26]. If we remove CP calibration from the workflow, we will not be able to predict how a patient *will likely* walk following a proposed treatment. However, if the goal is to determine how a patient *should* walk, CP calibration is no longer necessary, since the patient's control strategy is assumed to be changeable. For example, using CP values of 1 and no change in footpath, we recently predicted a novel gait pattern that successfully reduced both knee adduction torque peaks significantly when implemented in the gait laboratory by a single patient with knee OA [27].

When CP calibration is needed, there are several advantages to using quadratic response surfaces in place of repeated inner level optimizations. The primary advantage is computational speed. With this approach, the computational cost of the inner level optimizations is known in advance (64 runs) and paid only once up front. Furthermore, each inner level optimization can be performed in parallel on a different computer. Another important advantage is the ease with which the global minimum can be sought using either multiple gradient-based optimizations, as we did in this study, or a global optimizer. If one wishes to investigate the effect of optimization parameter settings (e.g., convergence tolerance, finite difference step size) on the solution, repeating the outer level optimization is computationally cheap with response surfaces.

The current version of our computational framework provides a variety of modeling alternatives. Model motion and ground reaction inputs to the inverse dynamics model can be parameterized using either the default B-spline nodes or polynomial plus Fourier coefficients [28]. The advantage of B-spline over polynomial-Fourier parameterization is that all of the design variables have similar magnitude, eliminating design variable scaling issues if finite difference gradients are used in the optimizations. However, use of automatic differentiation to create analytical gradients eliminates this scaling issue. A drawback of using B-spline nodes is that the lack of data points prior to the start and beyond the end of the cycle can create small kinematic oscillations resulting in control torque variations in the initial and final time frames.

We can also perform optimizations in two different simulation environments. Apart from our custom environment created using Matlab and C++, we can use the SIMM/Dynamics Pipeline environment (Motion Analysis Corporation, Santa Rosa, CA) to perform the same optimizations but without the computational benefits of automatic differentiation. Once the joint and inertial parameter cal-

ibration process is completed in phases one and two, we automatically create a SIMM joint file into which all of the optimized joint and inertial parameter values are written. An advantage of having a patient-specific joint file is that it facilitates animation of experimental and predicted gait motions. Apart from the lack of automatic differentiation, another disadvantage of the SIMM/Pipeline approach is the large amount of disk input/output required to run the executable repeatedly during an optimization, which greatly degrades performance.

The computational speed of our patient-specific modeling framework is already close to what would be needed for use in a clinical environment. Optimization of each isolated joint motion trial requires approximately 3 min of CPU time. The inertial parameter optimization requires less than 1 min. If joint and inertial parameters are optimized together using one cycle of gait data, the CPU time is on the order of 1 1/2 min. Each post-treatment predictive optimization using automatic differentiation requires approximately 10 min of CPU time. Finally, 1000 optimizations to calibrate control parameters using response surface approximations require roughly 10 min of CPU time. Computational speed was assessed on a 3.4 GHz Pentium 4 workstation with 2.00 GB of RAM.

In conclusion, we have developed a computational framework that can be used to predict a patient's post-treatment gait motion and loads given the patient's pre-treatment gait data. Our motivation for developing the framework is to improve planning of surgical and rehabilitation treatments for gait-related disorders. The ability to simulate new gait motions from a patient's pre-treatment gait data opens up exciting possibilities for improving the efficacy and reliability of clinical interventions. However, evaluation of the framework using a larger number of patients and wider variety of treatments is needed to assess its limitations and capabilities more fully.

## Acknowledgment

This work was supported by a Whitaker Foundation grant to B.J. Fregly.

## Conflict of interest

None of the authors of this manuscript have any conflict of interest related to this work.

## References

- [1] Andriacchi TP. Dynamics of knee malalignment. *Orthop Clin North Am* 1994;25(3):395–403.
- [2] Bryan JM, Hurwitz DE, Bach BR, Bittar T, Andriacchi TP. A predictive model of outcome in high tibial osteotomy. In: *Proceedings of the 43rd Annual Meeting of the Orthopaedic Research Society*, vol. 22. 1997. p. 718.
- [3] Hurwitz DE, Sumner DR, Andriacchi TP, Sugar DA. Dynamic knee loads during gait predict proximal tibial bone distribution. *J Biomech* 1998;31(5):423–30.
- [4] Prodromos CC, Andriacchi TP, Galante JO. A relationship between gait and clinical changes following high tibial osteotomy. *J Bone Joint Surg (American)* 1985;67(8):1188–94.
- [5] Wang J-W, Kuo KN, Andriacchi TP, Galante JO. The influence of walking mechanics and time on the results of proximal tibial osteotomy. *J Bone Joint Surg (American)* 1990;72(6):905–13.
- [6] Zhao D, Banks SA, Mitchell KH, D'Lima DD, Colwell CW, Fregly BJ. Correlation between the knee adduction torque and medial contact force for a variety of gait patterns. *J Orthop Res* 2007;25(6):789–97.
- [7] Mündermann A, Dyrby CO, Hurwitz DE, Sharma L, Andriacchi TP. Potential strategies to reduce medial compartment loading in patients with knee osteoarthritis of varying severity: reduced walking speed. *Arthritis Rheum* 2004;50(4):1172–8.
- [8] Andrews M, Noyes F, Hewett TE, Andriacchi TP. Lower limb alignment and foot angle are related to stance phase knee adduction in normal subjects: a critical analysis of the reliability of gait analysis data. *J Orthop Res* 1996;14(2):289–95.
- [9] Guo M, Axe MJ, Manal K. The influence of foot progression angle on the knee adduction moment during walking and stair climbing in pain free individuals with knee osteoarthritis. *Gait Posture*, in press.
- [10] Shaw JA, Moulton MJ. High tibial osteotomy: an operation based on a spurious mechanical concept. A theoretic treatise. *Am J Orthop* 1996;25(6):429–36.
- [11] Shaw JA, Dungey DS, Arshat SS. Recurrent varus angulation after high tibial osteotomy: an anatomic analysis. *Clin Orthop Relat Res* 2004;420(1):205–12.
- [12] Chao EYS. Graphic-based musculoskeletal model for biomechanical analyses and animation. *Med Eng Phys* 2003;25(3):201–12.
- [13] Chao EY, Sim FH. Computer-aided pre-operative planning in knee osteotomy. *Iowa Orthop J* 1995;15:4–18.
- [14] Reinbolt JA, Schutte JF, Fregly BJ, Haftka RT, George AD, Mitchell KH. Determination of patient-specific multi-joint kinematic models through two-level optimization. *J Biomech* 2005;38(3):621–6.
- [15] Leardini A, Cappozzo A, Catani F, Toksvig-Larsen S, Petitto A, Sforza V, et al. Validation of a functional method for the estimation of hip joint centre location. *J Biomech* 1999;32(1):99–103.
- [16] Bogert AJ van den, Smith GD, Nigg BM. In vivo determination of the anatomical axes of the ankle joint complex: an optimization approach. *J Biomech* 1994; 27(12):1477–88.
- [17] Anderson FC, Pandy MG. A dynamic optimization solution for vertical jumping in three dimensions. *Comput Methods Biomech Biomed Eng* 1999;2(3):201–31.
- [18] Bell AL, Pedersen DR, Brand RA. A comparison of the accuracy of several hip center location prediction methods. *J Biomech* 1990;23(6):617–21.
- [19] Churchill DL, Incavo SJ, Johnson CC, Beynon BD. The transepicondylar axis approximates the optimal flexion axis of the knee. *Clin Orthop Relat Res* 1998;356(1):111–8.
- [20] Inman VT. *The joints of the ankle*. Baltimore, Maryland: Williams and Wilkins Company; 1976.
- [21] de Leva P. Adjustments to Zatsiorsky-Seluyanov's segment inertia parameters. *J Biomech* 1996;29(9):1223–30.
- [22] Griewank A, Juedes D, Mitev H, Utke J, Vogel O, Walther A. ADOL-C: a package for the automatic differentiation of algorithms written in C/C++. *Assoc Comput Mach Trans Math Software* 1996;22(2):131–67.
- [23] Chéze L, Fregly BJ, Dimnet J. Determination of joint functional axes from noisy marker data using the finite helical axis. *Hum Mov Sci* 1998;17(1):1–15.
- [24] Hammersley J. Monte Carlo methods for solving multivariable problems. In: *Proceedings of the New York Academy of Science* 1960; 86:844–874.

- [25] Wada M, Imura S, Nagatani K, Baba H, Shimada S, Sasaki S. Relationship between gait and clinical results after high tibial osteotomy. *Clin Orthop Relat Res* 1998;354(1):180–8.
- [26] Reinbolt JA, Haftka RT, Chmielewski TL, Fregly BJ. Are patient-specific joint and inertial parameters necessary for accurate inverse dynamics analyses of gait? *IEEE Trans Biomed Eng*;54:782–793.
- [27] Fregly BJ, Reinbolt JA, Rooney KL, Mitchell KH, Chmielewski TL. Design of patient-specific gait modifications for knee osteoarthritis rehabilitation. *IEEE Trans Biomed Eng*, in press.
- [28] Nagurka ML, Yen V. Fourier-based optimal control of nonlinear dynamic systems. *J Dyn Syst Meas Control* 1990;112(1):17–26.